

An energy harvesting converter to power sensorized total human knee prosthesis

This content has been downloaded from IOPscience. Please scroll down to see the full text.

2014 Meas. Sci. Technol. 25 025702

(<http://iopscience.iop.org/0957-0233/25/2/025702>)

View [the table of contents for this issue](#), or go to the [journal homepage](#) for more

Download details:

This content was downloaded by: mauroserpelloni

IP Address: 192.167.23.210

This content was downloaded on 10/01/2014 at 07:59

Please note that [terms and conditions apply](#).

An energy harvesting converter to power sensorized total human knee prosthesis

V Luciano¹, E Sardini¹, M Serpelloni¹ and G Baronio²

¹ Department of Information Engineering, University of Brescia, Via Branze, 38, I-25123 Brescia, Italy

² Department of Mechanical Engineering, University of Brescia, Via Branze, 38, I-25123 Brescia, Italy

E-mail: mauro.serpelloni@ing.unibs.it

Received 12 November 2012, revised 15 October 2013

Accepted for publication 26 November 2013

Published 9 January 2014

Abstract

Monitoring the internal loads acting in a total knee prosthesis (TKP) is fundamental aspect to improve their design. One of the main benefits of this improvement is the longer duration of the tibial inserts. In this work, an electromagnetic energy harvesting system, which is implantable in a TKP, is presented. This is conceived for powering a future implantable system that is able to monitor the loads (and, possibly, other parameters) that could influence the working conditions of a TKP in real-time. The energy harvesting system (EHS) is composed of two series of NdFeB magnets, positioned into each condyle, and a coil that is placed in a pin of the tibial insert and connected to an implantable power management circuit. The magnetic flux variation and the induced voltage are generated by the knee's motion. A TKP prototype has been realized in order to reproduce the knee mechanics and to test the EHS performance. In the present work, the experimental results are obtained by adopting a resistive load of 2.2 k Ω , in order to simulate a real implanted autonomous system with a current consumption of 850 μ A and voltage of 2 V. The tests showed that, after 7 to 30 s of walking with a gait cycle frequency of about 1.0 Hz, the EHS can generate an energy of about 70 μ J, guaranteeing a voltage between 2 and 1.4 V every 7.6 s. With this prototype we can verify that it is possible to power for 16 ms a circuit having a power consumption of 1.7 mW every 7.6 s. The proposed generator is a viable solution to power an implanted electronic system that is conceived for measuring and transmitting the TKP load parameters.

Keywords: energy harvesting, electromagnetic generator, implantable sensor, autonomous device, knee prosthesis

(Some figures may appear in colour only in the online journal)

1. Introduction

A recent article [1] estimated that, among the candidates for total joint prosthesis, by 2016 there will be 50% more patients who are under 65 who will require a primary total knee replacement (TKR). On the other hand, the current duration of approximately 90% of TKPS is limited to 10 to 15 years [2] while life expectancy is increasing. Therefore, the revision TKR primary is a highly probable event with consequences related to surgery, such as pain, temporary inactivity, change of habits, etc [3, 4]. This leads to an increase in the cost of public health services [5]. The main causes of knee implant

revisions are the wear of the joint insert, which is made of ultra high molecular weight polyethylene (UHMWPE), and infections (osteolysis) due to total knee prosthesis (TKP) wear [6–8]. To reduce UHMWPE wear, it may be possible to better design prosthetic geometries that are in a close relationship with the surface shear stress and with UHMWPE wear [9]. These considerations justify the effort to better understand the dynamics and loads of TKP joint, which are very different from patient to patient over the course of a lifetime. Any technique that could ensure good knowledge of the load and, therefore, a better description of the system must be based on an *in vivo* real-time monitoring of the articular surface stress conditions

[10–14]. Therefore, a sensorized prosthesis that is capable of measuring *in vivo* parameters and which is able to identify the TKP conditions and to transmit the data outside the human body wirelessly could be a viable solution to this problem. Furthermore, physicians could continuously and remotely gather information to improve therapy and rehabilitation. For example, the center of pressure could be used to measure the collateral ligaments imbalance, indicating where the axial force applies more during a step cycle [15]. This leads to longer implant lifetime and better ease of use. Secondly, long-term benefits should be possible. In fact, the data coming from a large number of patients with different characteristics (age, gender, job, etc) could provide an invaluable source of information for a better in-depth prosthesis design. Since the possibility of powering the sensorized prosthesis with batteries cannot be prosecuted due to their limited life, the sensorized prosthesis must be autonomous; that is, able to provide itself with the necessary energy to make it function. The use of a power harvesting system that is suitable to generate the energy necessary for the functioning of a sensorized prosthesis would enable the system to work for the lifetime of the patient. Ideally, once it is implanted in the human body, it should not require any maintenance operation, at least from an energy point of view.

The present work aims to analyze and realize an electric generator prototype that is able to harvest the mechanical energy related to knee motion and convert it into electric energy so that it can supply power to a measurement circuit implanted in the TKP.

A number of different studies have proposed the harvesting of energy from human movements, particularly for electronic devices [16]. In [17], a device that exploits the knee movement using an oscillating device is presented. This device is optimized to be implanted in the prosthesis and the preliminary results show a total power output of about 850 μ W. In [18], Platt *et al* exploited piezoelectric ceramics implanted into an orthopedic prosthesis in order to monitor human knee activity. Each output of the three commercial piezoelectric elements was rectified and the unipolar output was stored in a 10 μ F capacitor. The whole implant generated 4.8 mW of raw electrical power. The overall electrical efficiency was about 19%. In [19], Chen *et al* draw on the work done by Platt *et al* and used four piezoceramic elements that were embedded into the implant, whose output power (about 1.2 mW) was adequate to supply the circuits of the TKR and to transmit the data to medical staff by RF signal. In [15], Almouahed *et al* designed and implemented a monitoring system of knee motion using piezoceramic elements, which were used as electrical energy harvesters and sensors. There are four piezoelectric elements between the femoral component and a custom-designed tibial component and, in this case, the generated electric power is supposed to supply circuits that implement several functions, including: acquisition, processing and transmission. By applying a load to each piezoceramic, the available power was estimated to be at most 1.8 mW for a single piezoceramic, so the total generated power was about 7.2 mW.

In this paper a different transduction principle is proposed. The described power harvesting system is based on a

direct conversion of the relative motion of tibia and femur, without motion or deformation of any other object, as commonly happens in other piezoelectric [15, 18, 19], inertial (electromagnetic or electrostatic [20]) or fluidic [21] energy harvesting systems (EHSs). This aspect allows the integration of the proposed EHS with less invasive alterations and reduced technical complications than the previous aforesaid EHSs. In particular, the piezoelectric EHSs must necessarily have a load that acts on the piezoelectric elements. Greater loads will generate greater amounts of charge. Meanwhile, the proposed transduction method requires no load to operate, it only requires a relative movement between the tibia and femur. This allows more fields of application with respect to the piezoelectric transduction. Furthermore, the piezoelectric transduction under quasi-static conditions of operation (excitation at low frequency) into useful energy presents considerable difficulties. Under these conditions, the piezoceramic generator is characterized by high-input capacitive impedance, low output current, and high output voltage. These characteristics are obviously unsuitable to directly power electronic components since the piezoceramic's ac output needs to be conditioned with a specific circuit. In this paper, the proposed electromagnetic system is connected to an energy management circuit that makes it possible to provide suitable levels of voltage and current for the power supply of an electronic circuit. Furthermore, in the proposed prototype, the absence of moving or buckling components reduces the risk of material failure. In fact, the electromechanical components are not in contact and are fixed in a dedicated housing. Consequently, they allow for a longer operating life span. In fact, the original implant modifications carried out are little and the prosthesis mechanical behavior is not modified, leaving the structurally weak parts almost unaltered. In particular, the modifications on the titanium femoral component do not change the prosthesis stiffness. The modifications on the polyethylene tibial tray are limited to the pin, which is not subject to high level of stress. All these aspects are essential for an implanted medical device. In [22, 23], preliminary considerations underlying the mechanical design of the system are described and a simple description of the first prototype is reported. Meanwhile, the overall design strategies and considerations of the proposed EHS are reported in this paper. Furthermore, a system prototype with an energy management circuit has been realized and tested. The reported experimental results confirm the possibility of autonomously supplying an implantable force-measurement circuit. In the following sections, the device's electromechanical aspects are discussed, the mechanical and electrical designs are then described and, finally, the experimental tests for measuring its performance are reported.

2. Design considerations

A TKP typically consists of three components: two elements cover the tibial and femoral epiphysis and a third element is interposed (figure 1(a)). The femoral component, which comprises two condyles is, generally, made of stellite (66% cobalt, 28% chromium, 6% molybdenum), the tibial

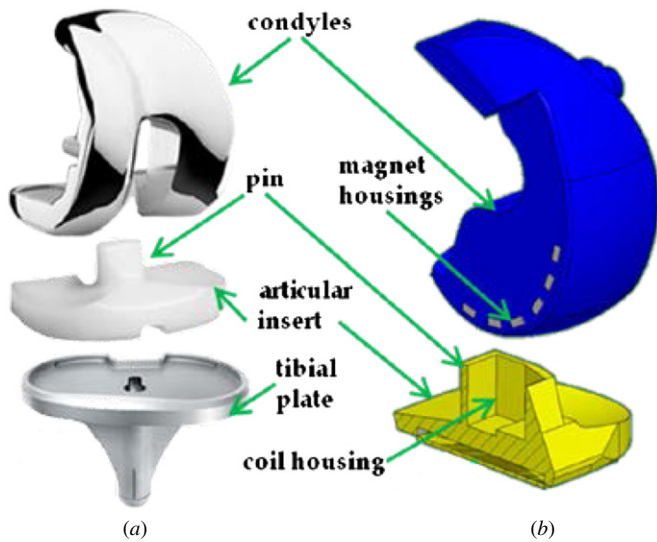


Figure 1. ZIMMER NexGen[®] Legacy[®] Knee LPS-Flex prosthesis (a), and vertical section of the realized CAD prosthesis prototype (b).

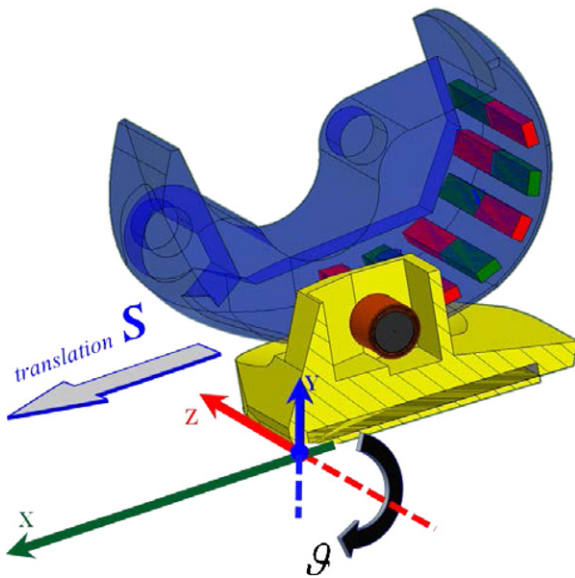


Figure 2. Sagittal section of the prosthesis with magnets and coil. Angle ϑ and translation S are the two degrees of freedom considered for simulating the real movement of a TKP.

component is a titanium alloy (but there are also models in stellite or polyethylene) and the articular insert is UHMWPE. The following analysis was conducted using a ZIMMER NexGen[®] Legacy[®] Knee LPS-Flex prosthesis (figure 1(a) [24]). This prosthesis is used for both primary and revision cases, and its design allows deep active flexions (up to 155°) with minimal loss of contact area and good stability. The prosthesis's real dimensions were obtained using a reverse engineering technique and used to design a 3D CAD model (figure 1(b)).

The EHS is composed of two series of six block-shaped magnets, with the magnetic axis parallel to the tibial plate, which are positioned into dedicated housings for each condyle. A cylindrical coil, parallel to the tibial plate, is placed in the

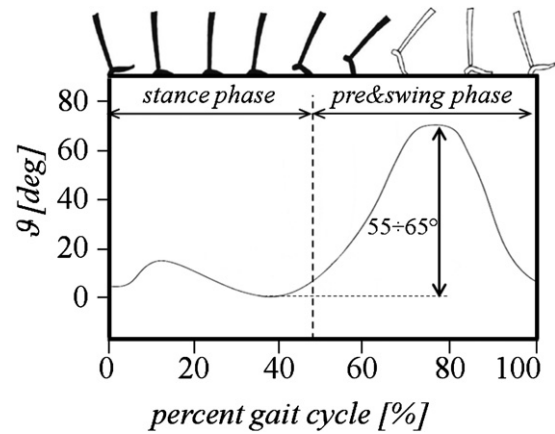


Figure 3. Gait cycle and knee joint flexion in the sagittal plane.

Table 1. Electromechanical component characteristics.

Component	Parameter (unit)	Value
Coil core	Material diameter;	NiZn ferrite 3.8, 13.6
	length (mm)	
Coil	Material diameter,	Cu (copper) 7.8, 13.6
	length (mm)	
	Number of turns	~3000
Magnet	Material width, length,	NdFeB 4, 2, 12
	height (mm)	
	Residual induction (mT)	1320–1380

polyethylene insert pin (figure 1(b)). The future measuring system will be conveniently placed in the UHMWPE insert, while the electronic circuit, for the storage and conditioning of the energy, is positioned in the pin (figure 1(b)). The dimensions and physical properties of the electromechanical components and the coil are reported in table 1.

The relative movement of tibial and femoral TKP inserts has six degrees of freedom and it is very complex. In particular, in the sagittal plane, the femur relative motion with respect to the tibia is not simply rotatory, a translational motion is also present.

The kinematical complexity of the problem has been approximated according to the following guidelines.

- (1) The degrees of freedom of the system have been reduced to only two, concerning the motion of the condyles in the sagittal plane, that is: rotation ϑ , representing the primary motion of the knee joint, and translation S , the only considered secondary motions of the knee (figure 2).
- (2) The gait cycle of the knee joint has been approximated as composed by two phases: the *stance phase* and the *swing phase*, during which, roughly, angle ϑ is $0^\circ < \vartheta_{\text{stance}} < 20^\circ$ and $0^\circ < \vartheta_{\text{swing}} < 60^\circ$ (figure 3), respectively.
- (3) Due to its longer time duration and mean velocity, only the swing phase has been considered significant from an energy point of view, $\vartheta_{\text{stance}}$ has then been supposed zero in the stance phase, while in the swing phase $0^\circ < \vartheta_{\text{swing}} < 60^\circ$.
- (4) In the swing phase the angular velocity is almost constant during the two rotations from $\vartheta_{\text{swing}} = 0^\circ$ to $\vartheta_{\text{swing}} = 60^\circ$ and back (figure 3).

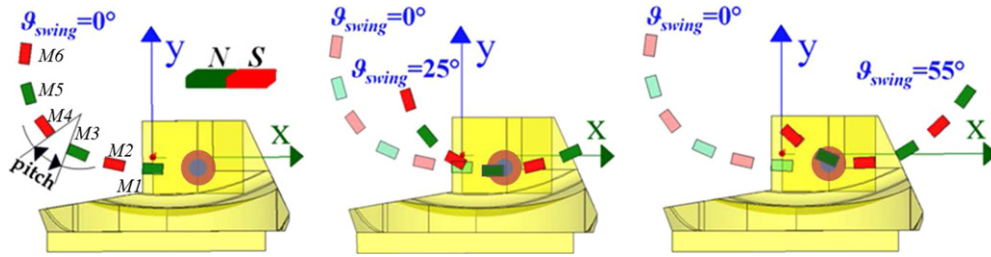


Figure 4. Relative positions of the magnets and the coil at different swing phase configurations. $M1, \dots, M6$ denote the six couples of magnets inserted in the condyles (not shown).

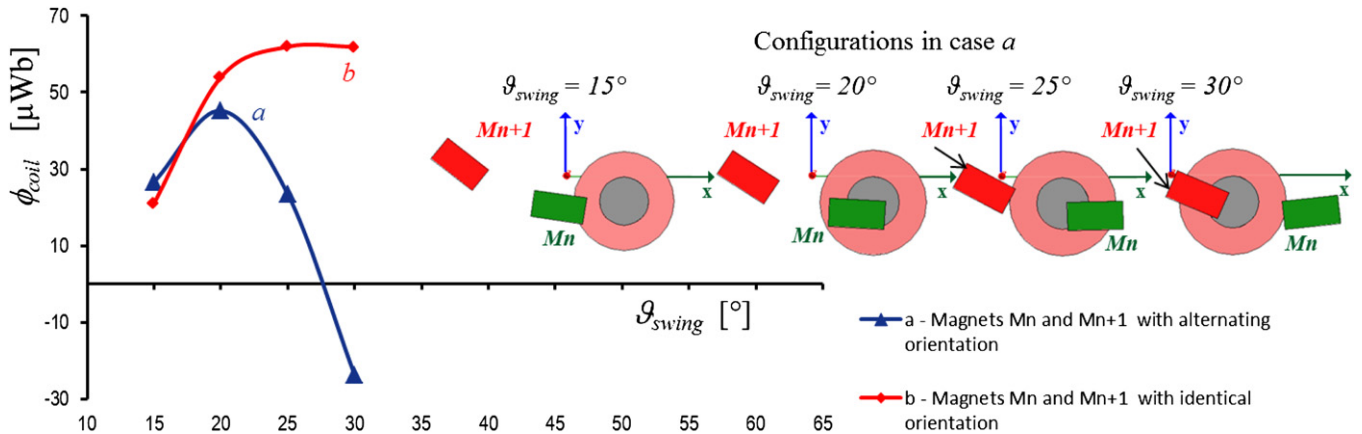


Figure 5. Simulation results obtained with Maxwell-3D (Ansoft) of the induced flux ϕ_{coil} in the interval $15^\circ \leq \vartheta_{swing} \leq 30^\circ$. Graphs *a* and *b* are referred to two following couples of magnets, M_n and M_{n+1} , with different magnetic orientations. On the right corner M_n and M_{n+1} have alternating orientation (case *a*).

(5) On average, the anterior–posterior translation S of the condyles, with respect to the tibial insert, has been fixed at about 10 mm [25–27].

During the gait, the relative motion of tibia and femur produces a variable magnetic flux in the coil, generating an electromotive force, according to the Faraday–Neumann–Lenz’s law.

A basic equation that describes the phenomena is:

$$V_i = -n \frac{d\phi_{coil}}{dt} = -n \frac{d\phi_{coil}}{d\vartheta} \cdot \frac{d\vartheta}{dt}, \quad (1)$$

in which t is the time, $\phi_{coil} = \phi_{coil}(\vartheta)$ is the induced flux on the coil in each single angular configuration ϑ , and n the number of turns of the coil.

Equation (1) shows that the induced voltage depends on the characteristics of the gait ($d\vartheta/dt$) and on the variability of the flux ϕ_{coil} with the angle ϑ ($d\phi/dt$). Referring to figure 3, V_i can be considered close to zero when the gait is in the stance phase and close to its greatest value in the swing phase; that is, when the angular velocity $d\vartheta/dt$ executes a rotation from 0° to 60° and back. Since the rising and decreasing curves of figure 3 during the swing phase can be approximated by two straight lines, $d\vartheta/dt$ can be replaced by two constant values, approximately equal to 240° s^{-1} and $-240^\circ \text{ s}^{-1}$.

To increase the V_i value, a possible strategy in this paper has been pursued by building a row of magnets so as to create contiguous space regions of great magnetic variation and to place the coil in order to intercept this magnetic variation. The relative position of the coil with respect to the row of magnets

has been optimized by simulating the complex trajectories of the row.

The position of the row of magnets as a function of angle ϑ has been simulated using a tailored Matlab[®] program. Figure 4 shows the magnet positions $M1$ to $M6$ with respect to the coil for three different ϑ during the swing phase. Considering figure 4, let be M_n ($n = 1, \dots, 6$) the generic couple of magnets, symmetrically disposed with respect to the x – y plane. In this way, the first magnet crossing the coil, when the swing phase starts, is $M1$.

Another geometrical parameter that influences the flux variability with respect to ϑ is the pitch (figure 4); that is, the interval between two following magnets together with the coil diameter. Each magnet has been chosen so as to have a dimension equal to the coil diameter. The distance between two following magnets is almost equal to the width of each magnet. In this way, each magnet roughly begins its coil crossing when the magnet (preceding it) begins to exit from the coil.

A finite element simulation with the software Maxwell-3D, marketed by Ansoft, was implemented to evaluate the flux variation when each magnet of the row is opposite or concordant with next one. In figure 5, the induced flux produced by two following couples of magnets in the interval $15^\circ \leq \vartheta_{swing} \leq 30^\circ$ for two different magnetic dipole orientations (alternating in case *a* and identical in case *b*), as a function of the ϑ angle, is shown.

This result has been obtained using a computation method exposed in a similar finite element simulation, as discussed in a previous work [22]. From figure 5, it is clear how the relative

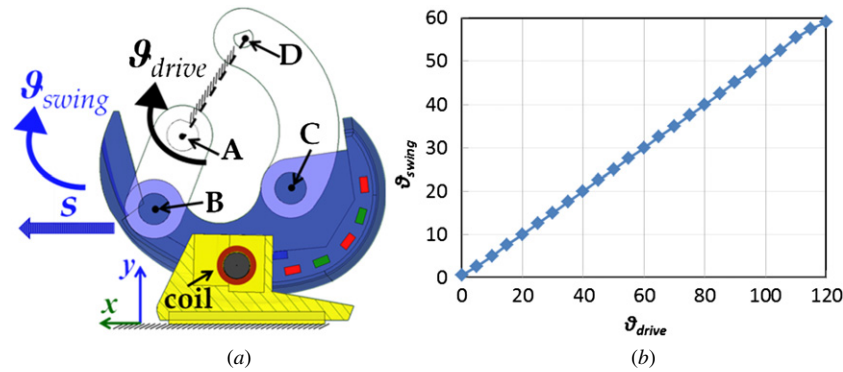


Figure 6. (a) Four-bar mechanism and kinematic parameters used for simulations and tests of TKP joint motion in (sagittal) x - y plane. (b) Relationship between ϑ_{swing} and ϑ_{drive} .

polarity of two following couples of magnets influences the ratio $d\phi_{coil}/d\vartheta_{swing}$. In particular, a bigger variability of ϕ_{coil} exists in the case of magnets disposed with alternating polarity (graph *a*). In the simulated interval, the slope of graph *a* is about 270% bigger than for *b*. However, it is possible to repeat the same observations for the other intervals.

3. Knee prosthesis prototype

The goal of the developed EHS is to supply a measurement circuit implanted in a TKP; such as, an implantable autonomous force sensor (IAFS), which can measure and transmit the measured data wirelessly outside the human body. To verify this possibility, the energy level of the electromechanical generator has been evaluated by building a prototype, reproducing the ZIMMER NexGen® Legacy® Knee LPS-Flex prosthesis, that is equipped with magnets and coil, and which is able to reproduce the knee movement in order to measure the energy produced.

An analysis on the TKP kinematics during normal walking activity has been conducted assuming the approximation discussed in section 2. This analysis led to the design of the four-bar mechanism ABCD, as shown in figure 6(a).

The variability range for angle ϑ and translation S has been chosen considering points (2), (3) and (5) of section 2. In particular, the linkage analysis has been deduced by different papers in the literature, considering a range of motions in the sagittal plane that patients with TKP are likely to experience during different daily activities [28–30].

In figure 6(a), link AB is the input crank, rotating with the angle ϑ_{drive} about point A. Link BC is the rod rotating with angle ϑ_{swing} . Angle ϑ_{swing} is the condyles rotation with respect to reference x - y system of the tibial insert. Finally, point D is the rotation center of driven link CD, and AD is the frame of the four-bar linkage, fixed in the reference x - y system. Figure 6(b) shows the relationship between ϑ_{swing} and ϑ_{drive} . This relationship can be approximated as linear with a $\frac{1}{2}$ slope. The angular velocities are in the same proportion.

Using the 3D CAD model, which was previously introduced, the results from the four-bar mechanism analysis has been used to build a knee prosthesis prototype using rapid prototyping technology (i.e. fused deposition modeling



Figure 7. Photograph of the realized TKP prototype.

Table 2. Characteristics of the comfortable speed walking (c.s.w.) gait cycle considered in the tests.

Gait cycle parameters (unit)	Comfortable speed walking (c.s.w.)
Velocity (m s^{-1})	1.27
Cadence (steps min^{-1})	121.6
Stride length (m)	1.25
Maximum flexion during swing (ϑ_{swing_max}) ($^{\circ}$)	55.45
Frequency of walk cycle (Hz)	1.016

process). A photo of the developed apparatus is shown in figure 7.

The prototype has been driven in a way to simulate a gait cycle compatible by TKP patients and which we have named comfortable speed walking (c.s.w.) [31]. The characteristics of the c.s.w. gait are reported in table 2.

The ϑ_{drive} has been driven assuming that for the stance phase at point (3) of section 2; that is, the angular velocity during the time T_{stance} is imposed zero. Meanwhile, in the swing phase two opposite rotations are present; that is, ϑ_{swing} is

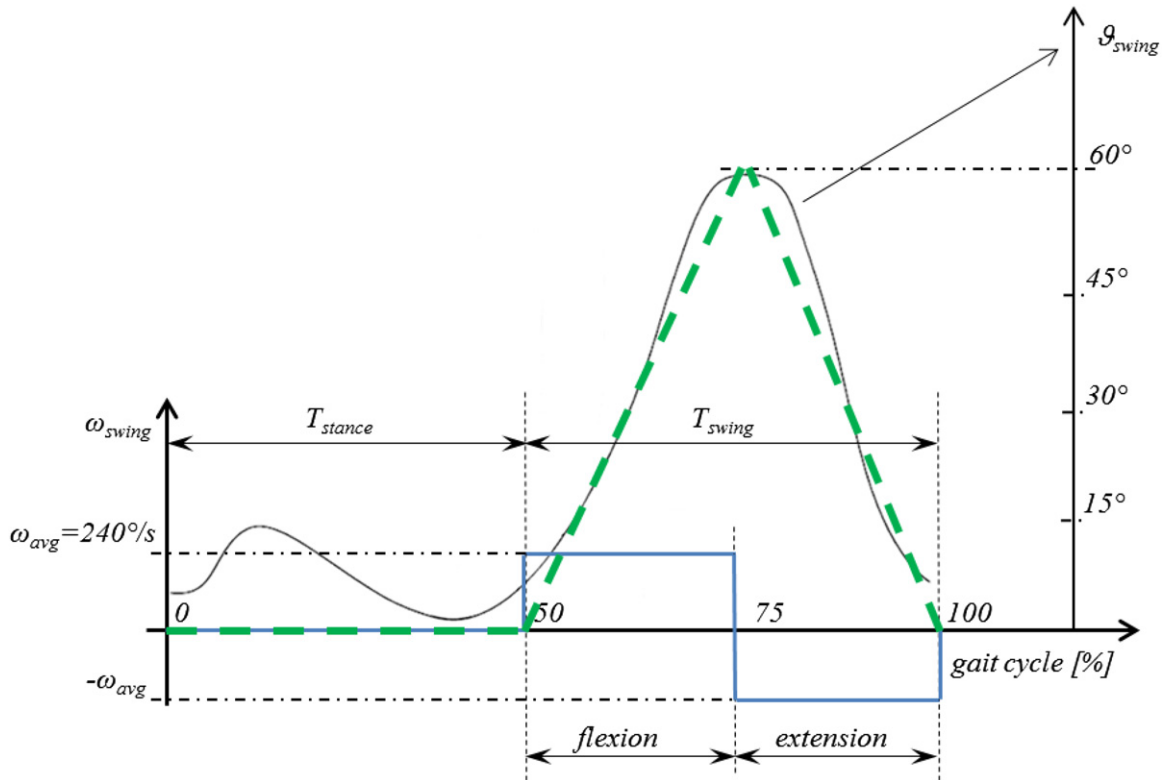


Figure 8. Trend of imposed angular velocity ω_{swing} during the tests reproducing the c.s.w. gait conditions in blue. The effective angular variation in green dashes and in black the trend of the angular variation as reported in figure 3.

variable from 0° to 60° (approximately) during flexion and back during extension (figure 3).

The flexion and the extension phases are half of the gait cycle (T_{cycle}). In these phases, the gait cycle has roughly a linear trend, which allows the angular velocity and equal to the mean value ω_{avg} to be constant.

Figure 8 reports the imposed angular velocity in blue on ω_{swing} , the supposed angular variation in green obtained by the stepper motor’s motion controller, and in black the trend of the angular variation of the c.s.w. as reported in figure 3.

The step motor was driven using high acceleration/deceleration ramps ($35\,700\text{ rad s}^{-1}$ [32]), obtaining a very high response time compared to the $T_{flexion}$ and $T_{extension}$ time and justifying the angular velocity trend outlined in figure 8. The previous analysis completely defines the input kinematical parameters for the following tests.

The motion control system, used for activating the prototype, is in open loop. It consists of a programmable drive (RTA PLUS K5, [32]) with dedicated PC based motion controller, and a stepper motor (Sanyo Denki, model 103–H7823–1740, [32]) with basic step angle $1.8^\circ \pm 0.09^\circ$ and theoretical acceleration $35\,700\text{ rad s}^{-2}$.

The experimental layout is outlined in figure 9.

The EHS electrical performance, as described below, has been tested by first measuring the generator open circuit voltage $V_{o.c.}$, and by subsequently connecting the generator output to an electronic circuit that is able to manage the produced energy and to power supply a load with a voltage V_L and a current I_L .

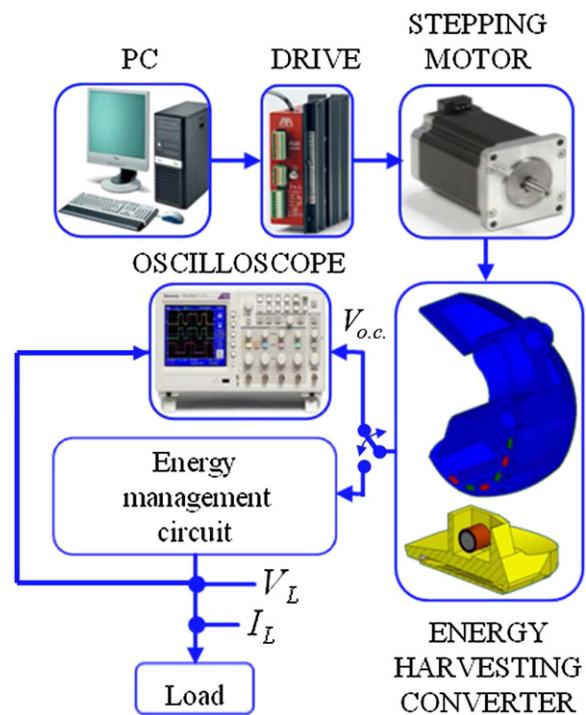


Figure 9. Schematic representation of the experimental setup.

4. Discussion and results

Figure 10 reports the measured open circuit voltage $V_{o.c.}$ during the comfortable walking speeds that are given in table 2.

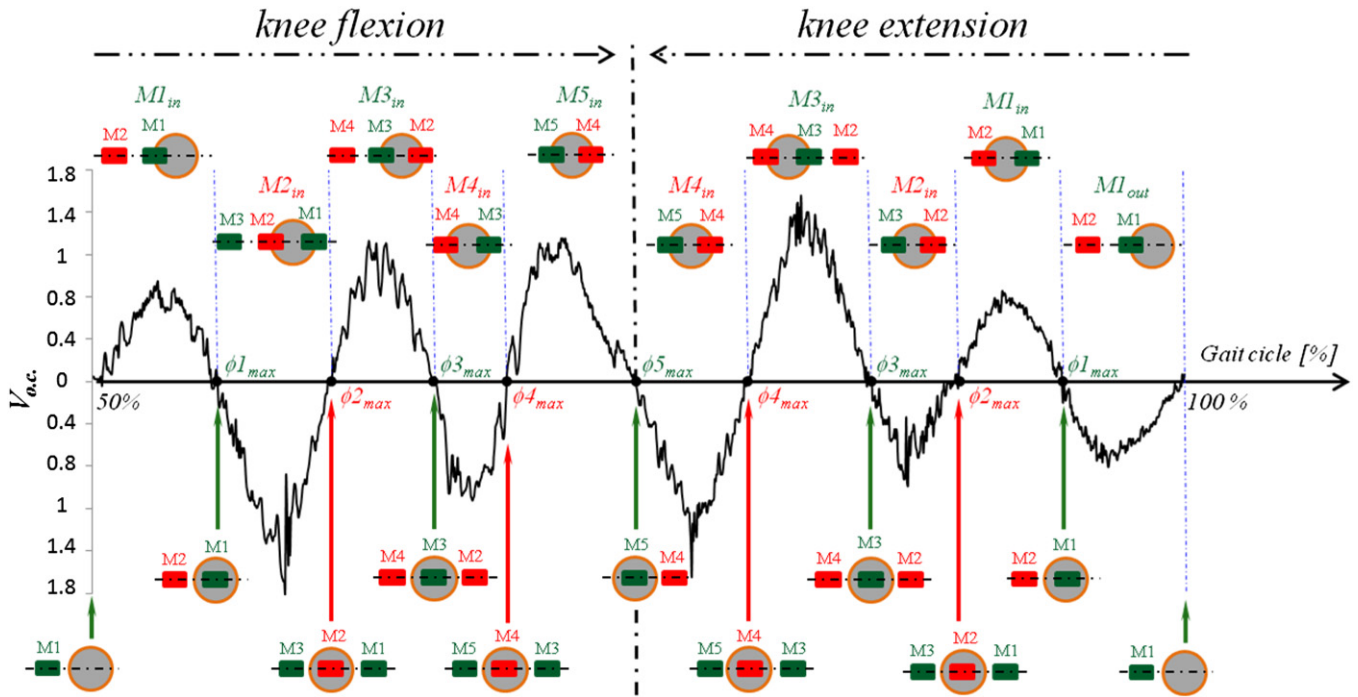


Figure 10. The measured open circuit voltage $V_{o.c.}$ during swing phase laboratory reproduction (gait cycle frequency = 1.0 Hz). Symbols $M1_{in}, \dots, M5_{in}$ are time intervals during which magnets $M1, \dots, M5$ cross the coil (see also figure 4), and arrive at positions, $\phi1_{max}, \dots, \phi5_{max}$, in which induced flux is max (zeros of induced voltage). $M1_{in}$ and $M1_{out}$ are time intervals during which $M1$ goes from its initial position to $\phi1_{max}$ and vice versa.

This graph shows that an open circuit voltage has a trend oscillating with sufficient regularity and is in good agreement with the variability of the flux obtained, for this situation, from a simulation performed in a previous work [22]. Furthermore, it is possible to make a simple comparison between the results of simulation of figure 5 with the experimental results of figure 10 by applying equation (1). With the magnetic flux variation calculated by simulation and the number of turns of table 1, a variation of the induced voltage of about $3 V_{pp}$ is calculated. This value corresponds to the experimental value of about $2.5 V_{pp}$, which can be deduced from figure 10. The lower value could be due to dissipation factors.

For clarity of representation, in figure 10 the magnets and the coils are reported along a (dotted) straight line, although its trajectories are curvilinear. In the stance phase (roughly half gait cycle) the voltage is zero since the imposed movement is zero. Therefore, only the voltage measured in the swing phase is shown. Symbols $M1_{in}, \dots, M5_{in}$ represent the magnets $M1, \dots, M6$ and their position with respect to the coil for a specific gait position.

In figure 10, $M6$ does not contribute to the voltage generation since it does not compare in front of the coil due to the characteristics of the chosen gait. In addition, although the flux is obviously induced by all of the magnets, due to the rapid attenuation with the distance of the magnetic induction field intensity the whole flux can be considered as induced mainly by the couple of magnets whose orthogonal projection on the $x-y$ plane (figure 4) crosses the coil. For this reason, the minimum and maximum points $\phi_{n_{max}}$ of induced flux are outlined in the lower part of figure 10 with complete projection across the

coil of the representative magnets, subscript n indicating the magnets Mn giving the bigger part of the total flux.

The EHS operating performance has been evaluated by connecting a load that is equivalent to a force measuring circuit implanted inside the prosthesis. In [33], a TKP with an IAFS system was developed. The power consumption of the IAFS, for gait conditions similar to the c.s.w., was 1.7 mW for a data acquisition and transmission cycle during about $T_{IAFS} = 13$ ms. Consequently, a total energy $E_L = 22.1 \mu J$ was necessary for the functioning of the system. In the present work, the experimental results are obtained adopting a resistive load $R_L = 2.2 k\Omega$ in order to simulate the IAFS current consumption of $850 \mu A$ with a power supply voltage of 2 V.

Since the power produced by the proposed generator is not sufficient to uninterruptly supply the IAFS, a tailored electronic circuit is necessary to adapt the harvested energy to the load energy requirements. Figure 11 shows a schematic representation of the principal elements of the circuit that has been designed, realized and used for the tests.

In this circuit, the first step is to rectify the sinusoidal signal from the generator. Then, the management circuit, which is a commercial component Seiko S-882Z for ultra-low voltage operations, permits us to store the energy on the capacitor $C_{start-up}$, increasing the voltage V_C . Although the load is always connected to the management circuit, the power supply is erogated only when the voltage V_C reaches $2.0 V (V_{out_1})$ and it continues until the stop voltage value of $V_C = 1.4 V (V_{out_2})$.

In correspondence of V_{out_2} , the control disconnects the load from the start-up capacitor (time L-off in figure 12).

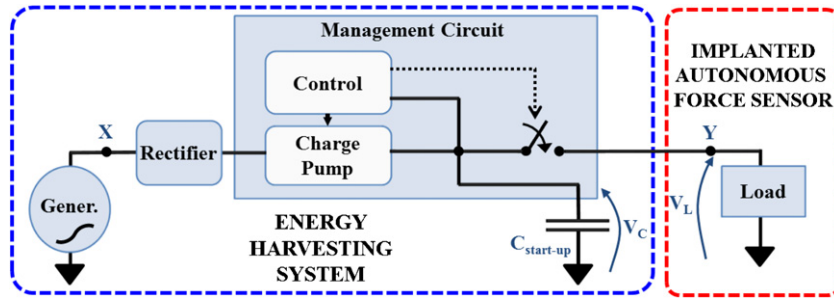


Figure 11. Schematic representation of main elements of the circuit used for tests.

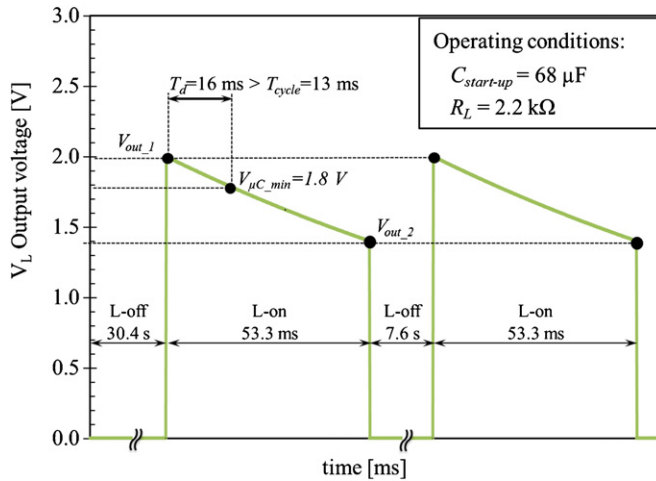


Figure 12. Output voltage V_L when connected to a resistive load R_L exploited to reproduce the power consumption of the implantable autonomous force sensor.

An appropriate choice of capacitance $C_{\text{start-up}}$ of the start-up capacitor was obtained considering that, for a proper operation, the IAFS requires an energy of about $E_L = 22.1 \mu\text{J}$ with a minimum supply voltage $V_{\mu\text{C_min}} = 1.8 \text{ V}$.

Under operating conditions that emulate the operation of the IAFS, an energy of about $E_L = 22.1 \mu\text{J}$ is ensured and a discharge time $T_d = 16 \text{ ms}$, greater than $T_{\text{IAFS}} = 13 \text{ ms}$, is necessary to V_L output voltage to decrease from V_{out_1} to $V_{\mu\text{C_min}}$ (figure 12).

The physical effort that the patient can be requested to do in order to allow the system to function can be summed up in two states. Starting from zero initial conditions (i.e. when initial voltage of start-up capacitor is zero), the start-up capacitor charging time is $T_{c,\text{zic}} = 30.4 \text{ s}$ (figure 13). Meanwhile, starting from steady state conditions (i.e. when initial start-up capacitor voltage is equal to V_{out_2}) the charging time is $T_{c,\text{ssc}} = 7.6 \text{ s}$ (figure 13). This means that the EHS is able to supply the IAFS with an energy of about $E_L = 26 \mu\text{J}$, guaranteeing a tension between 2 and 1.8 V every 7.6 s.

Using the relation $E_L = 0.5 \cdot C_{\text{start-up}} [(V_{\text{CPout}_1})^2 - (V_{\mu\text{C_min}})^2]$ a minimum value $C_{\text{start-up}} = 58 \mu\text{F}$ can be calculated. The chosen $C_{\text{start-up}}$ of $68 \mu\text{F}$ makes available, during L-on, a level of energy of about $70 \mu\text{J}$, of which just $22 \mu\text{J}$ are used by the circuit while the remaining $50 \mu\text{J}$ are wasted since the voltage is less than the circuit operating voltage and V_{out_2} is fixed by the commercial component.

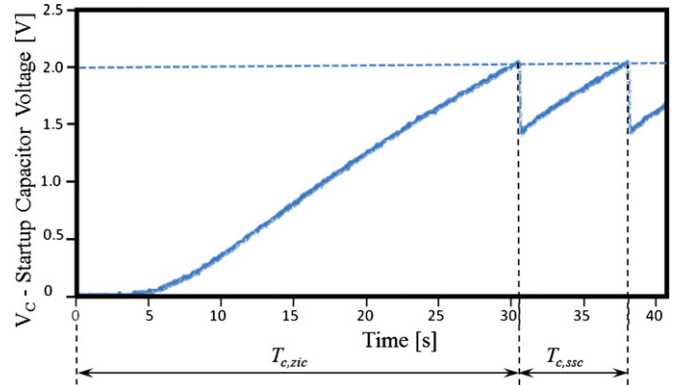


Figure 13. Typical CP output voltage trend, measured using a $68 \mu\text{F}$ start-up capacitor, during continuous operating conditions of EHS and starting from zero initial conditions.

The circuit's efficiency has been calculated as the ratio between the output power measured on the load in point Y (figure 11) and the input power applied to the rectifier input, (pointed as X again in figure 11 and without any connection to the generator). The experimental energy efficiency is about 10%. Thus, the management circuit generates an output power that is equal to $70 \mu\text{J}$ over an energy of about $700 \mu\text{J}$ provided by the electromagnetic generator in the interval L-on. Since the management circuit requires 7.6 s to recover the energy level, the power generated during the comfortable speed walking is about $92 \mu\text{W}$.

In both situations (i.e. $T_{c,\text{zic}} = 30.4 \text{ s}$ and $T_{c,\text{ssc}} = 7.6 \text{ s}$), the gait time requested to the patient to charge the start-up capacitor is acceptable. In the tested conditions, the performance of proposed EHS is sufficient to ensure the proper operation of IAFS.

As a general consideration, an appropriate choice of $C_{\text{start-up}}$ can also make it possible to supply a circuit implanted in the prosthesis to measure different quantities.

5. Conclusions

In this work an energy harvesting system (EHS) that is based on an electromagnetic converter has been studied, developed and tested.

The proposed solution has been conceived with the aim of powering a measuring circuit implanted in a knee prosthesis. The EHS consists of a row of magnets, a coil and a tailored power management circuit for energy conditioning and storing.

This has been tested by connecting to a load simulating the behavior of a force measuring system that has been implanted in the knee prosthesis. The tests successfully demonstrate the possibility to power the implantable force sensor system and to transmit the prosthesis measurement data. The energy to supply the measurement to execute a single force acquisition and transmission outside the human body is harvested for a walking gait cycle frequency of about 1.0 Hz. At the start-up the system is powered after walking roughly 30 s, while in the steady condition it is powered every 7.6 s. A lot of energy is wasted due to the limitations of commercial components used in the management circuit and a strong reduction of the recharging time (now 7.6 s) in the steady condition. It is feasible to reduce this to about 1 s; for example, by providing a change in the stop voltage value of 1.4 V up to 1.8 V. This means that a one gait cycle can be used to recharge and one gait can be used to measure.

The EHS is a viable solution to power an electronic circuit aimed at measuring other quantities than the force implantable in a knee prosthesis. Future analysis will be focused on a more accurate reproduction of the geometry of the system and the kinematics of a total knee prosthesis in order to achieve a higher miniaturization of the components and to improve the efficiency of the energy harvester, which is about 10% in the present state of the art. Improving this parameter opens the possibility to greatly increase the activity of the measuring circuit.

References

- [1] Kurtz S M, Lau E, Ong K, Zhao K, Kelly M and Bozic K J 2009 Future young patient demand for primary and revision joint replacement: national projections from 2010 to 2030 *Clin. Orthop. Relat. Res.* **467** 2606–12
- [2] Austin M S, Sharkey P F, Hozack W J and Rothman R H 2004 Knee failure mechanisms after total knee arthroplasty *Tech. Knee Surg.* **3** 55–9
- [3] Saleh K J, Dykes D C, Tweedie R L, Mohamed K, Ravichandran A, Saleh R M, Gioe T J and Heck D A 2002 Functional outcome after total knee arthroplasty revision: a meta-analysis *J. Arthroplasty* **17** 967–77
- [4] Saleh K J, Rand J A and McQueen D A 2003 Current status of revision total knee arthroplasty: how do we assess results? *J. Bone Joint Surg. Am.* **85** (Suppl 1) S18–20
- [5] Kayode O O, Diarmuid C M, Ray J W, Simi P B and Kevin J M 2010 Increasing financial burden of revision total knee arthroplasty *Knee Surg. Sports Traumatol. Arthrosc.* **18** 915–18
- [6] Mortazavi S M J, Molligan J, Austin M S, Purtill J J, Hozack W J and Parvizi J 2011 Failure following revision total knee arthroplasty: infection is the major cause *Int. Orthop.* **35** 1157–64
- [7] Bozic K J, Kurtz S M, Lau E, Ong K, Chiu V, Vail T P, Rubash H E and Berry D J 2010 The epidemiology of revision total knee arthroplasty in the United States *Clin. Orthop. Relat. Res.* **468** 45–51
- [8] Heimke G, Leyen S and Willmann G 2002 Knee arthroplasty: recently developed ceramics offer new solutions *Biomaterials* **23** 1539–51
- [9] Essner A, Herrera L, Hughes P and Kester M 2011 The influence of material and design on total knee replacement wear *J. Knee Surg.* **24** 9–17
- [10] Almouahed S, Hamitouche C, Stindel E and Roux C 2008 New trends in instrumented knee prostheses *3rd Int. Conf. on Information and Communication Technologies: From Theory to Applications* pp 1–6
- [11] Kirking B, Krevolin J, Townsend C, Colwell C W Jr and D’Lima D D 2006 A multiaxial force-sensing implantable tibial prosthesis *J. Biomech.* **39** 1744–51
- [12] Graichen F, Arnold R, Rohlmann A and Bergmann G 2007 Implantable 9-channel telemetry system for *in vivo* load measurements with orthopedic implants *IEEE Trans. Biomed. Eng.* **54** 253–61
- [13] Morris B A, D’Lima D D, Slamin J, Kovacevic N, Arms S W, Townsend C P and Colwell C W Jr 2001 e-Knee: evolution of the electronic knee prosthesis. Telemetry technology development *J. Bone Joint Surg. Am.* **83** (Suppl 2) 62–6
- [14] Kondo M, Fujii T, Kitagawa H, Tsumura H and Kadoya Y 2008 Arthroscopy for evaluation of polyethylene wear after total knee arthroplasty *J. Orthop. Sci.* **13** 433–37
- [15] Almouahed S, Gouriou M, Hamitouche C, Stindel E and Roux C 2011 The use of piezoceramics as electrical energy harvesters within instrumented knee implant during walking *IEEE/ASME Trans. Mechatronics* **16** 799–807
- [16] Mitcheson P D, Yeatman E M, Rao G K, Holmes A S and Green T C 2008 Energy harvesting from human and machine motion for wireless electronic devices *Proc. IEEE* **96** 1457–86
- [17] Turri S and Benbouzid M E H 2009 Preliminary study of a pendulum *in vivo* electromechanical generator for orthopedic implants *Proc. IECON: 35th Annual Conf. of the IEEE and ICELIE, 3rd IEEE Int. Conf. on E-Learning in Industrial Electronics* pp 4415–4420
- [18] Platt S, Farritor S, Garvin K and Haider H 2005 The use of piezoelectric ceramics for electric power generation within orthopedic implants *IEEE/ASME Trans. Mechatronics* **10** 455–61
- [19] Chen H, Liu M, Jia C and Wang Z 2009 Power harvesting using PZT ceramics embedded in orthopedic implants *IEEE Trans. Ultrason. Ferroelectr. Freq. Control* **56** 2010–14
- [20] Baginsky I, Kostsov E and Sokolov A 2010 Electrostatic microgenerators of energy with a high specific power *Optoelectron. Instrum. Data Process.* **46** 580–92
- [21] Wang D A and Chang K H 2010 Electromagnetic energy harvesting from flow induced vibration *Microelectron. J.* **41** 356–64
- [22] Luciano V, Sardini E, Serpelloni M and Baronio G 2012 Analysis of an electromechanical generator implanted in a human total knee prosthesis *Proc. IEEE Sensors Applications Symp. (7–9 February, Brescia)* pp 1–5
- [23] Baronio G, Luciano V, Sardini E and Serpelloni M 2013 Design considerations of an electromechanical generator implanted in human total knee prosthesis *Int. J. Mechatronics Manuf. Syst.* **6** 270–84
- [24] www.zimmer.com/content/pdf/en-US/NexGen_LPS_Flex-Fixed_Brochure_%2897-5964-101%29.pdf
- [25] Iwaki H, Pinskerova V and Freeman M A 2000 Tibiofemoral movement I: the shapes and relative movements of the femur and tibia in the unloaded cadaver knee *J. Bone Joint Surg. Br.* **82** 1189–95
- [26] Pinskerova V, Johal P, Nakagawa S, Sosna A, Williams A, Gedroyc W and Freeman M A 2004 Does the femur roll-back with flexion? *J. Bone Joint Surg. Br.* **86** 925–31
- [27] Pinskerova V, Iwaki H and Freeman M A R 2000 The shapes and relative movements of the femur and tibia at the knee *Der Orthopäde* **29** (Suppl 1) S3–5
- [28] McClelland J A, Webster K E and Feller J A 2009 Variability of walking and other daily activities in patients with total knee replacement *Gait Posture* **30** 288–95

- [29] Jevsevar D S, Riley P O, Hodge W A and Krebs D E 1993 Knee kinematics and kinetics during locomotor activities of daily living in subjects with knee arthroplasty and in healthy control subjects *Phys. Ther.* **73** 229–39
- [30] Hatfield G L, Hubley-Kozey C L, Wilson J L A and Dunbar M J 2011 The effect of total knee arthroplasty on knee joint kinematics and kinetics during gait *J. Arthroplasty* **26** 309–18
- [31] McClelland J A, Webster K E, Feller J A and Menz H B 2011 Knee kinematics during walking at different speeds in people who have undergone total knee replacement *The Knee* **18** 151–5
- [32] www.rta.it/doc/PLUS_K_ita.pdf
- [33] Crescini D, Sardini E and Serpelloni M 2011 Design and test of an autonomous sensor for force measurements in human knee implants *Sensors Actuators A* **166** 1–8